2019 International Conference on Robotics and Automation (ICRA)
Palais des congres de Montreal, Montreal, Canada, May 20-24, 2019

Design and Parameter Optimization of a 3-PSR Parallel Mechanism for Replicating Wave and Boat Motion

Kurt Talke[1,2], Dylan Drotman[2], Nicholas Stroumtsos[1], Mauricio de Oliveira[2], Thomas Bewley[2]

***Abstract*— We present a low-cost, three-degree-of-freedom (3-DOF) prismatic-spherical-revolute (PSR) parallel mechanism used as a testing platform for an unmanned aerial vehicle (UAV) tethered to an unmanned surface vehicle (USV). The mechanism has three actuated linear rails kinematically linked to a platform which replicates boat motion up to 2.5 m vertical heave (sea state 4, Douglas Sea Scale). A lookup table relating relative slider heights to platform roll and pitch was developed numerically leveraging geometric constraints. A design parameter study optimized the arm length, platform size, and ball joint mounting angle relative to the overall radius to maximize the workspace. For this design, a maximum roll and pitch range from -32° to 32° and -25° to 35°, respectively, is achievable. A prototype was manufactured to carry the tethered UAV winch payload. Experimental testing confirmed the workspace and demonstrated boat motion replication, validated using an inertial measurement unit (IMU).**

I. Introduction

The operation of an unmanned air vehicle (UAV) connected to a small unmanned surface vehicle (USV) via a semi-slack tether, as shown in Fig. 1, presents challenges due to the ocean dynamics affecting the control of the system [1]. To develop a winch-based system to manage a semi-slack tether's dynamics and oscillations, a repeatable testing environment is needed for replicating open water dynamics and boat motion. A testing platform capable of replicating wave and boat motion allows for land-based testing, reducing costs and the design iteration cycle time. The alternative, of relying on weather conditions to test in specific sea states is too costly, time limiting, and dangerous.

The development of the parallel six degree of freedom (6-DOF) Gough-Stewart platform in the 1960s sparked a wealth of research into wave and boat motion simulation and replication. Originally developed for simulating flight [2] and tire testing [3], the platform has been used in a variety of applications, including telescope positioning [4], cnc machining [5], precision surgery [6], wave compensation [7], wave energy conversion [8], [9], and floating platform replication for UAV landing [10]. To carry heavy loads, the designs often use a hydraulic piston, which have limited range of extension. The high cost and limited motion from hydraulic pistons limits the capabilities of existing systems, usually resulting in mechanisms that are scaled down. This can be problematic if trying to capture the full heave, or vertical translation displacement of boat motion in large waves. Some 6-DOF and 4-DOF prismatic-spherical-spherical (6-PSS, 4-PSS) mechanisms on parallel linear rails have been proposed to achieve larger displacements, but not for wave replication [11–13]. Other ship motion replication mechanisms decouple heave from orientation, using lifts to capture the full scale range of vertical motion, but are large and costly [14]. Manmade wave pools, like Naval Surface Warfare Center (NSWC) Carderock's Manuevering and Seakeeping (MASK) basin have been used for replicating waves [15], [16]. These wave replication systems are very expensive to build and use. Often, they are specifically built for recreation and limited to less than 1.25 m waves [17]. There is no existing low-cost system that can capture the full scale range of heave for moderate to high sea states.

For the coordinated UAV-USV scenario, USV motion can

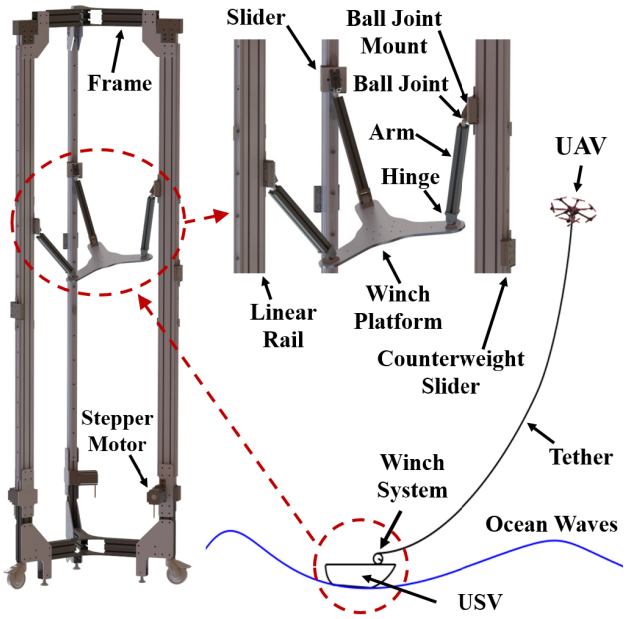

Fig. 1: Conceptual 3-PSR parallel mechanism for wave and boat motion replication. The sliders on the vertical rails are kinematically linked to the platform, and actuated to replicate the roll, pitch and heave motion experienced by an USV. This specific mechanism is designed for testing a winch controller for a tethered UAV-USV system.

[1]These authors are with Space and Naval Warfare Systems Center Pacific, Unmanned Systems Advanced Development group, San Diego , CA 92110, USA kurt.talke@navy.mil, nicholas.stroumtsos@navy.mil

[2]These authors are with the Dept. of MAE, MC 041, UC San Diego La Jolla, CA 92093, USA ddrotman@ucsd.edu, mauricio@ucsd.edu, bewley@ucsd.edu

Support for this work was provided by Space and Naval Warfare Systems Center Pacific under the Naval Innovative Science and Engineering program, Naval Research Enterprise Internship Program, and the Department of Defense SMART Scholarship for Service program.

be characterized by three orientation DOFs {roll, pitch, yaw} and three translation DOFs {heave, surge, sway}. The dominant DOFs of the USV induced by sea waves are roll, pitch, heave. The other three DOFs {surge, sway, yaw} change at a slower rate, are an order of magnitude smaller, and are often induced by propellers, wind, and currents [18]. Any drift of the minor DOFs motion are more easily gradually corrected by the UAV-USV system. Thus, a reduced 3-DOF mechanism, which has control in the primary DOFs {roll, pitch, heave} is sufficient to capture the major motions of the USV in high sea states. That motion can be accounted for via feedback control applied to the winch system for reliable operation.

Many 3-DOF prismatic-revolute-spherical (3-PRS) and revolute-prismatic-spherical (3-RPS) parallel mechanisms have been proposed and thoroughly analyzed [19–26]. However, these mechanisms don't provide the desired control in the primary DOFs for wave replication {roll, pitch, heave}, with minimal coupling of the minor DOFs {surge, sway, yaw}. By switching the location of the joints, thus creating a 3-DOF prismatic-spherical-revolute (3-PSR) parallel mechanism, we can achieve the desired mobility and control. Specifically, the 3-PSR design allows for large displacement heave and precise control of 2 orientation DOFs {roll, pitch}.

This paper presents the design of a novel, low-cost, 3-PSR parallel mechanism capable of replicating the full scale range of boat heave up to sea state 4. A design parameter optimization maximized the roll-pitch workspace. A three-axis interpolation approach is presented to accurately generate a desired path through the roll-pitch workspace. The 3-PSR parallel mechanism was fabricated and experimentally validated using an inertial measurement unit (IMU).

The remainder of the paper is organized as follows. Section II details the design and hardware selection. Section III derives the relevant geometric constraints to develop the kinematic lookup table. Section IV details and discusses the roll-pitch workspace. Section V discusses the design parameter optimization approach and results. Section VI discusses the interpolation of the lookup table. Section VII investigates the generation of motion profiles and discusses the experimental results. Section VIII summarizes the key conclusions.

II. Design

A 3-PSR parallel mechanism is proposed to replicate the primary DOFs {roll, pitch, heave} for wave replication, similar to one developed for a shipboard stabilization platform [27]. The proposed design, as shown in Fig. 1 does not require a redundant fourth link which differentiate it from previous work. The proposed design uses linear guides to achieve the required heave range for sea state 4.

A. Mechanical Design

To accommodate the large displacement required in the vertical direction, three rails with belt driven actuated sliders are used as prismatic joints. The sliders are attached to three arms through spherical ball joints. The arms then connect to a platform through revolute hinge joints. The platform is large enough to carry the winch system, and can roll and pitch at any height along the vertical rails by changing the relative slider heights according to the workspace lookup table derived in Section IV. The radially symmetric equilateral design limits an UAV to 120° of operating space. Similar to an elevator, a secondary slider system acts as a counterweight to ease the static torque requirements of the actuators and prevent catastrophic damage in the event of a failed motor. Low-cost stepper motors allow for a motion profile to be commanded in open loop.

A primary benefit of this design and the following analysis is the ability to scale the design for larger wave heights. By extending the vertical rails, the heave range can be increased. Larger payloads can be achieved by increasing the radius, arm length, and platform size. A higher torque motor can be easily integrated to account for a heavier payload. This design works well in applications where heave is a major component of the required motion, an order or two greater. The platform can be oriented up from the sliders instead of down, which would be beneficial for perfecting the automated landing of an UAV.

TABLE I: Prototype Hardware

Hardware	Supplier	Part Number
T-slotted frame	MiniTec	Profile 45x90 F
Linear rail + slide	MiniTec	LR6S + LR6
Timing belt pulley	MiniTec	28.0510/1
Stepper motor	Anaheim Automation	34Y214S-LW8
Motor driver	Anaheim Automation	MBC10641
Micro-controller	Azteeg	X3
Power supply	B&K Precision	9117
Ball joint	Mcmaster	8412K120
Hinge	MiniTec	21.2020
Firmware	Custom	-

B. Hardware

An experimental prototype was developed using T-slotted extruded aluminum for the frame, fabricated large enough to replicate wave conditions up to 2.5 m heave (sea state 4), with a 5 to 15 second period [28]. A geared belt system was used driven by NEMA 34 stepper motors with a maximum torque of 8.5 N-m, enough to carry a 15 kg payload on the platform. Stepper motor drivers capable of 10 A at 80 V were required to fully use the torque range of the motors. A 3D printer micro-controller based off the Arduino ATMEGA 2560 communicates with the stepper motor drivers. Custom firmware was developed to command motor steps per clock tick, running at 10 Hz. Table I lists the specific hardware used. All hardware was purchased for under $6k USD.

III. Kinematics

The kinematic derivations in the literature on 3-PSR parallel mechanisms are limited, primarily due to the challenge of determining coupling DOFs of the platform for typical inverse kinematic approaches. A previous 3-PSR

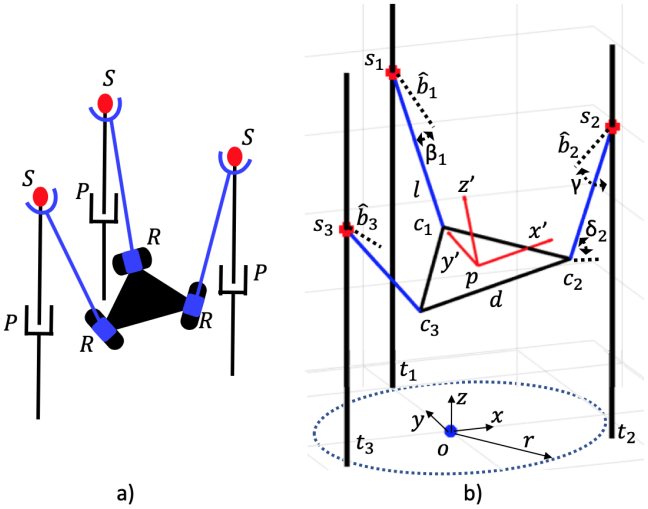

Fig. 2: 3-PSR mechanism schematic. a) Diagram of the linkage structure. b) Design parameters for solving kinematics.

mechanism derived an inverse mapping between the platform and sliders under the assumption that the platform location and orientation are known [27]. They first determined the coupling of the translation DOFs {surge, sway} to determine the platform location when orientation DOFs {roll, pitch} are independently specified. They then use screw theory to solve for the required slider heights. However, they neglect the induced coupling of the orientation DOF {yaw} when two orientation DOFs {roll, pitch} are specified jointly. To reiterate, knowing two orientation DOFs {roll, pitch} does not immediately give the position of corners of the platform for typical inverse kinematic approaches. Because the third orientation DOF {yaw} coupling can not be solved analytically when two orientation DOFs {roll, pitch} are specified, a forward kinematic numerical procedure to develop a lookup table is considered here.

A. Geometric and Hinge Constraints

Given slider heights for the schematic shown in Fig. 2, the spatial coordinates of the corners of the platform can be solved using geometric constraints and hinge constraints for each of the three towers. The distance between the platform corner and slider is defined as:

$$||s_i - c_i|| = l \tag{1}$$

where s_i are the coordinates of the slider for the i'th tower, c_i are the coordinates of the i'th corner of the platform, and l is the constant length of the arm. A similar geometric constraint equation specifies the size of the platform:

$$||c_i - c_j|| = d \tag{2}$$

where c_j are the coordinates of the j'th corner and d is the edge length of the equilateral shaped platform. The hinge joint constrains the arm to be perpendicular to the back edge of the platform. When perpendicular, the inner product of the vector from the slider to the corner of the platform and the back edge is zero:

$$\langle s_i - c_i, c_j - c_k \rangle = 0 \tag{3}$$

where c_k are the coordinates of the k'th corner of the platform.

Combining Eq. 1, Eq. 2, and Eq. 3 for each of the three towers leads to a system of 9 equations with 9 unknowns. The nine unknowns are the x, y, and z coordinates of the three platform corners. This set of equations can be solved with a numerical solver such as the Newton-Raphson (NR) method for any given set of slider heights [29].

B. Platform Pose

The location of point p, roll, pitch, yaw, hinge, and ball joint angles can be determined knowing the x, y, and z locations of the three corners of the platform. Point p, defined as the center of mass (COM) of the platform, is found from the mean of the x, y, and z coordinates of the corners. The coupled surge, sway, and heave of the platform correspond to the translation of point p. The body coordinate vectors, x', y', and z' define an affine rotation matrix from a unit length coordinate system centered at the origin of the world frame, o. The platform normal vector is found from the normalized cross product of two of the edges.

$$z' = \frac{(c_1 - c_3) \times (c_1 - c_2)}{||(c_1 - c_3) \times (c_1 - c_2)||} \tag{4}$$

The remaining platform body coordinate vectors are found from the normalized vector between corner 1 and point p,

$$y' = \frac{(c_1 - p)}{||(c_1 - p)||} \tag{5}$$

and the cross product of y' and z'.

$$x' = y' \times z' \tag{6}$$

The roll, pitch, and yaw angles can be backed out from three seperate entries of the 1-2-3 Tait Bryan rotation matrix [30]:

$$\phi = \arcsin z'^{(1)} \tag{7}$$

$$\theta = -\arcsin \frac{z'^{(2)}}{\cos\phi} \tag{8}$$

$$\psi = -\arcsin\left(\frac{y'^{(1)}}{\cos\phi}\right) \tag{9}$$

where ϕ is roll, θ is pitch, ψ is yaw, and the 1 and 2 superscripts correspond with the first and second entry of the respective vector. The i'th hinge angle, δ_i, is found from the normalized inner product of the arm vector with the vector from the respective corner to point p:

$$\delta_i = \arccos \frac{\langle c_i - p, s_i - c_i \rangle}{||c_i - p|| l} \tag{10}$$

The i'th ball joint angle, β_i, is found from the normalized inner product between the arm vector and the mounting axis as:

$$\beta_i = \arccos \frac{\langle s_i - c_i, \hat{b}_i \rangle}{l} \tag{11}$$

where $\hat{b}_i$ is the unit length mounting axis of the ball joint defined by:

$$\hat{b}_i = R(\gamma)\,\hat{t}_i \tag{12}$$

where γ is the ball joint mounting angle and $\hat{t}_i$ is the unit length vector from the origin to the base of the tower. $R(\gamma)$ is a rotation matrix to rotate the vector by the ball joint mounting axis angle:

$$R(\gamma) = \begin{bmatrix} 1 & 0 & 0 \\ 0 & \cos\gamma & -\sin\gamma \\ 0 & \sin\gamma & \cos\gamma \end{bmatrix} \tag{13}$$

The equations defined here provide the precise platform pose required to define the workspace for parameter optimization.

IV. Workspace

We first investigated the workspace for nominal, nondimensional length parameters, i.e., the tower radius, $r = 1$, arm length, $l = 1$, and platform edge length $d = 1$, and then used the results to optimize these design parameters in Section V. All possible combinations of relative slider heights were simulated apriori to develop a lookup table relating platform pose to slider heights. To capture the entire workspace, the first slider was kept at a height of $2.5r$, and the other two ranged from 0 to $5r$ in 200 increments. For each combination of slider heights, the geometric constraints were solved numerically from Eq. 1, Eq. 2, and Eq. 3 using the tower base coordinates as initial guesses for the NR method. When a numerical solution was found, the roll and pitch angles were calculated using Eq. 7 and Eq. 8.

A. Physical Constraints

Two physical constraints are applied to avoid mechanical singularities. First, the platform must physically stay within the towers. The arm vectors must never be parallel with the towers, imposed by only keeping solutions where the inner product between the arm vector and tower vector is greater than 0.

$$\langle s_i - c_i, \hat{t}_i \rangle \geq 0 \tag{14}$$

Secondly, the arm can not rotate through the platform, limiting the hinge range from 0° to 180°. This is imposed by only keeping solutions where the inner product between the arm vector and platform normal are greater than 0.

$$\langle s_i - c_i, z' \rangle \geq 0 \tag{15}$$

B. Workspace Results

We first present the workspace for the nominal parameters as shown in Fig. 3a. As the design is symmetric across the y-z plane, the workspace is symmetric across the $\phi = 0$ axis. The slider curves, defining the movements of the three sliders, wrap back in on themselves in the regions near the boundaries and corners of the workspace. These regions of kinematic lock corresponds to an extreme platform orientation that can only be achieved after a specified set of slider movements. More specifically, after the platform moves to the boundary of the workspace, it can move back away from the boundary by yawing. The curves stop when the physical constraints are applied, where the mechanism would become singular.

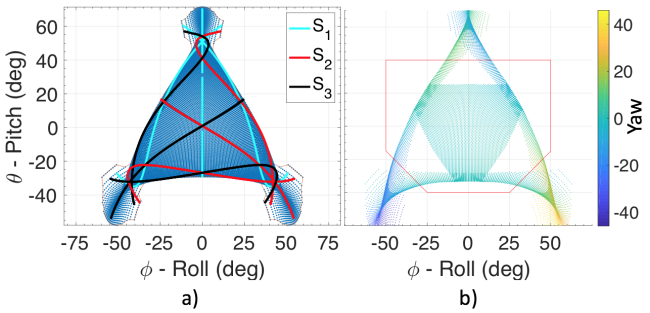

Fig. 3: Roll - pitch workspace for: a) Nominal design parameters $r = l = d = 1$. The S_1, S_2, and S_3 curves correspond to the path through the space by changing one of the slider heights while keeping the other two constant. The three curves for each slider path correspond to different relative slider heights of the other two sliders. b) Sub-optimal design parameters $r = 1$, $l = 1.1$, and $d = 1.15$. Yaw coupling is shown by the color intensity map. The missing area results from imposing the physical constraints. The roll - pitch workspace inside the polygon was maximized in the parameter optimization.

The yaw coupling, as shown in Fig. 3b for sub-optimal design parameters, is largest at the extreme roll and pitch angles and regions near the edge of the boundary. The coupling is different for the same roll and pitch combinations in these regions as seen by the overlapping color intensities. Imposing the physical constraints can potentially leave holes, or disjoint regions in the workspace. These regions represent where the platform would have to travel outside the towers, or the hinge would rotate past 180°, through a mechanical singularity, and potentially invert the platform.

The coupling of the two uncontrollable translation degrees of freedom have similar results, but are not shown. Surge is symmetric across the $\phi = 0$ axis, while sway is inversely symmetric across the same axis. The maximum translation coupling is ∼50% of the nominal scale. For this application, where heave motion is significantly greater than the nominal scale, the yaw, surge and sway coupling are within an acceptable negligible range.

V. Design Parameter Optimization

An engineering objective is to find the design parameters which maximize the workspace given the geometric and physical constraints. A parameter study was performed varying l and d relative to r from 50% to 150% in 2.5% increments. For each parameter combination, the area of the boundary of the workspace was calculated. The parameter sets with disjointed workspace were discarded. The regions of kinematic lock at the corners of the workspace were reduced by limiting the hinge angle range from 26° to 180°. This was enforced by normalizing Eq. 15 and keeping solutions greater than or equal to .45:

$$\frac{\langle s_i - c_i, z' \rangle}{||\langle s_i - c_i, z' \rangle||} \geq .45 \approx \cos(90° - \delta_i) \tag{16}$$

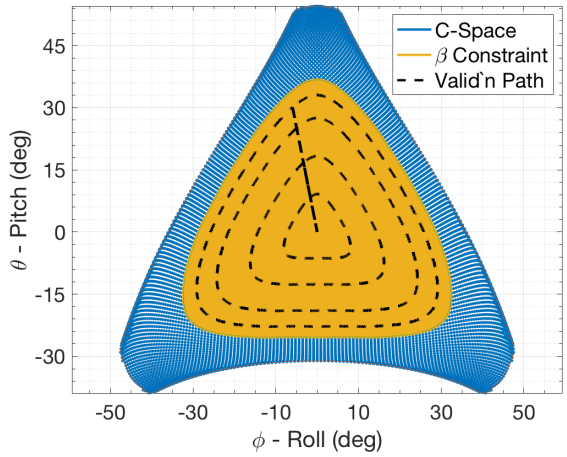

Fig. 4: Maximized workspace after parameter optimization. The larger region shows the workspace optimization for design parameters $r = 1$, $l = 0.825$, and $d = 1.325$. The smaller region shows the workspace for design parameters $r = 1$, $l = 0.975$, $d = 1.15$, and $\gamma = 30^\circ$ given the ball joint constraint. The motion profile for the workspace validation experiment is shown by the dashed line

To further remove the regions of kinematic lock from the optimization, the boundary of the workspace was intersected with the polygon shown in Fig. 3b. The area of the intersection was then calculated for all parameter combinations and the maximum found.

A. Ball Joint Mounting Angle

The ball joint used in the prototype is capable of 30° rotation in all directions. For each design parameter set in the nominal optimization, the ball joint axis angle was varied from 20° to 45° in 1° increments. The area of the resulting workspace was calculated such that all ball joint angles within the workspace were less than the physical limit.

B. Parameter Optimization Results

The scale of this optimization resulted in ∼70 million numerical solves of the system of nine equations, which proved computationally intensive. To speed up the process, the optimization was performed on a supercomputer, running all 41 possible combinations of the arm length parameter in parallel. The optimal workspace for both the nominal optimization and the ball joint mounting angle optimization are shown in Fig. 4. The regions of kinematic lock have been minimized, and there are no disjoint regions. The region for the ball joint constraint is $\sim 60\%$ of the overall workspace. The roll and pitch range achievable is from -32° to 32° and -25° to 35°, respectively. Table II catalogs the top six

TABLE II: Top 6 maximum workspace parameters

Rank	1	2	3	4	5	6
Area $(^\circ)^2$	4551.9	4547.1	4543.1	4540.9	4536.8	4535.7
l	0.825	0.85	0.875	0.9	0.925	1.05
d	1.325	1.3	1.275	1.25	1.225	1.1

TABLE III: Top 6 maximum workspace parameters given the ball joint constraint

Rank	1	2	3	4	5	6
Area $(^\circ)^2$	2816.5	2813.9	2812.7	2811.5	2809.2	2805.1
l	0.975	1.0	1.0	0.95	1.0	1.0
d	1.15	1.075	1.125	1.075	1.05	1.1
$\gamma\,(^\circ)$	30	32	30	34	33	31

parameters and workspace area. The arm length and platform size change inversely proportional to each other as the area slightly decreases. Table III catalogs the top six parameters given the ball joint angle constraint and workspace area.

VI. Path Generation

A simple way to generate a path through the workspace for simulation and experimentation is to use a high fidelity lookup table with ∼1000 increments between the minimum and maximum slider heights. Such a lookup table results in ∼.1° resolution in roll and pitch. For ∼1000 increments between 0 and $5r$, the slider resolution between points is proportional to the nominal scale as $.005r$. Depending on the scale, this may be much larger than the position accuracy of the stepper motors. Interpolation of the lookup table can improve the accuracy of path generation.

A. Three Axis Interpolation

A three-axis interpolation approach, as shown in Fig. 5, is required to determine s_i^*, the commanded slider heights. Given a desired roll-pitch combination, w_d, the nearest roll-pitch point, w_n, is determined by subtracting w_d from all workspace combinations, $w_{(i,j,k)}$, and finding the minimum value. The vector from w_n to w_d, is projected onto each of the slider motion directions using the inner product. The final slider height for each slider i is determined by adding a scaled, proportional amount of the projection to the slider height, s_i^n corresponding to w_n:

$$s_i^* = s_i^n + \frac{2}{3}\sum_{m=1}^{3} \frac{||\langle w_d - w_n, w_m - w_n\rangle||}{||w_m - w_n||}\Delta h_m \qquad (17)$$

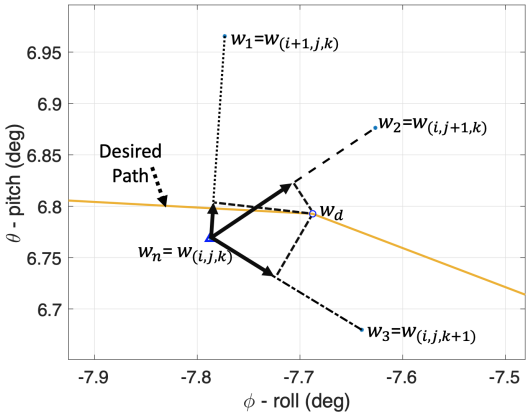

Fig. 5: Three-axis interpolation approach. The vector from the desired point to the nearest point is projected onto the three directions of motion, then proportionally added to each slider height.

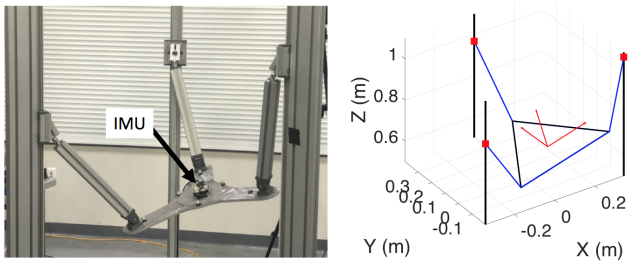

Fig. 6: Workspace validation. a) Prototype mechanism during workspace motion profile testing. An IMU at the center captures the platform pose. b) Matlab simulator for the same motion profile. Both show near identical pose.

where Δh_m is the slider height change between w_m and w_n. The slider motion profile is then numerically differentiated using a fourth order central difference method to command slider velocity [29].

VII. Experimental Validation

A prototype was built using the optimal parameters in Table III, scaled up to the minimum size to accommodate an UAV winch payload, resulting in $r = 0.40$ m, $d = 0.46$ m, and $l = 0.39$ m. Fig. 6 shows the prototype during testing next to a Matlab simulation showing the same pose. Because the design uses stepper motors and runs in open loop, motion profiles and corresponding slider heights were determined apriori using the three-axis interpolation of the lookup table. Two motion profiles were considered: a profile to validate the workspace and a boat motion profile. Both motion profiles were validated using an inertial measurement unit (IMU).

A. Workspace Validation Profile

To test the entire workspace, the ball joint constraint boundary was offset by 25%, 50%, 75%, and 90%. These were connected as the desired motion profile, as seen by the connected level sets path shown in Fig. 4. The commanded height of the sliders was adjusted such that the COM had no commanded heave.

Fig. 7a shows a typical result from the workspace motion profile. After adjusting for the initialization offset and starting time, the IMU coincides with the commanded profile

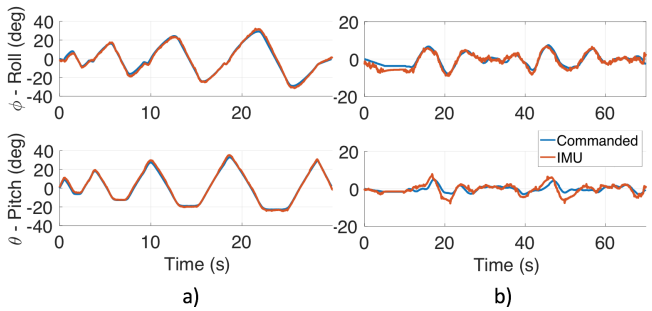

Fig. 7: Experimental results showing the platform orientation vs. time for a typical trial of the a) Workspace motion profile and b) Wave motion profile. The blue curve is the commanded path, and the red curve the output from the IMU.

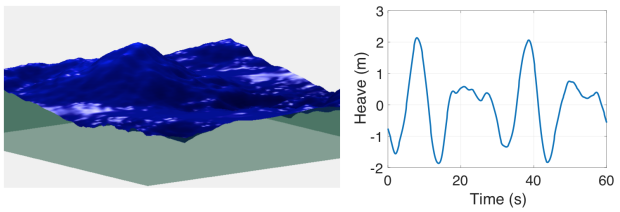

Fig. 8: Input wave data for the mechanism. a) Numerical simulator for waves up to sea state 4. b) Corresponding boat heave profile.

well. The average error for roll and pitch was 1.2° with a standard deviation of 2.8°. Note that yaw, not shown, is coupled, but remained below 5°.

B. Boat Motion Profile

An open-source numerical ocean simulator based on the Phillips spectrum was used for generating wave data [31–35]. Fig. 8 shows the numerical simulator along with the specified heave profile. Simulating boat motion in rough waves, or converting known ocean motion to boat motion is a challenging problem [36], [37]. A simplification, used here, is to assume the orientation of the boat is fixed to three separate points on the wave surface, making a plane. From this plane, the specified roll, pitch, and heave can be backed out using a similar calculation to Eq. 7, and Eq. 8.

Fig. 7b shows a typical result from the wave motion profile. The roll and pitch are seen to follow the commanded paths. The average error for roll and pitch was 1.2° with a standard deviation of 3.1°. The errors in pitch, seen around 20 and 50 seconds can be attributed to spikes in the commanded slider steps, found only after testing. The root cause was linked to the data output from the numerical wave simulator. We are confident that using better input data would negate these errors. The vibrations from the stepper motors as slower speeds may have added to the noisier signal.

VIII. Conclusion

In this paper, a 3-PSR parallel mechanism was presented, capable of replicating spectral based ocean wave and boat data for testing a winch system for a tethered UAV. Geometric constraint equations were derived to build a lookup table given the position of the vertical sliders. A parameter optimization resulted in a roll-pitch workspace suitable for replicating ocean waves up to sea state 4. A three-axis interpolation method of the lookup table was presented for more accurate motion profile generation. Experiments were conducted using an IMU to verify the workspace and a wave profile. Experimental results show an error between the actual and desired motion of $\leq 2°$. This ocean wave and boat motion replicator design is low-cost, and easily scale-able for different payload sizes and wave heights. It can be adapted to other use cases by scaling the design parameters and actuator hardware according to the parameter optimization results. We plan to mount a prototype winch system to simulate how boat motion affects tether dynamics.

REFERENCES

[1] K. Talke, T. Bewley, and M. Oliveira, "Tether shape analysis for a uav - usv team," in *2018 IEEE International Conference on Intelligent Robots (IROS)*, Oct 2018.

[2] D. Stewart, "A platform with six degrees of freedom," *Proceedings of the Institution of Mechanical Engineers*, vol. 180, no. 1, pp. 371–386, 1965.

[3] V. Gough, "Universal tyre test machine," *Proc. FISITA 9th Int. Technical Congr., London, 1962*, pp. 117–137, 1962.

[4] J. C. Jáuregui, E. E. Hernández, M. Ceccarelli, C. López-Cajún, and A. García, "Kinematic calibration of precise 6-dof stewart platform-type positioning systems for radio telescope applications," *Frontiers of Mechanical Engineering*, vol. 8, pp. 252–260, Sep 2013.

[5] Y. Ting, Y.-S. Chen, and H.-C. Jar, "Modeling and control for a gough-stewart platform cnc machine," *Journal of Robotic Systems*, vol. 21, no. 11, pp. 609–623, 2004.

[6] M. Wapler, V. Urban, T. Weisener, J. Stallkamp, M. DÃŒrr, and A. Hiller, "A stewart platform for precision surgery," *Transactions of the Institute of Measurement and Control*, vol. 25, no. 4, pp. 329–334, 2003.

[7] W. De Zeeuw, "Ship motion compensation platform for high payloads; dynamic analysis and control," 2012.

[8] A. L. Madsen, "Design of stewart platform for wave compensation," Master's thesis, Aalborg Universitet, Denmark, 2012.

[9] B. Lotfi and L. Huang, "A novel wave energy converter using the stewart platform," *Journal of Green Engineering*, vol. 4, pp. 33–48, 2014.

[10] A. Campos, J. Quintero, R. Saltaren, M. Ferre, and R. Aracil, "An active helideck testbed for floating structures based on a stewart-gough platform," in *2008 IEEE/RSJ International Conference on Intelligent Robots and Systems*, pp. 3705–3710, Sept 2008.

[11] Y. Ye and W. Chen, "Frequency- and time-domain analysis of a multi-degree-of-freedom point absorber wave energy converter," *Advances in Mechanical Engineering*, vol. 9, p. 168781401772208, 12 2017.

[12] W. Xu, Y. Li, and X. Xiao, "Kinematics and workspace analysis for a novel 6-pss parallel manipulator," pp. 1869–1874, 12 2013.

[13] F. Gao, W. Li, X. Zhao, Z. Jin, and H. Zhao, "New kinematic structures for 2-, 3-, 4-, and 5-dof parallel manipulator designs," *Mechanism and Machine Theory*, vol. 37, no. 11, pp. 1395 – 1411, 2002.

[14] J. Jansen, R. Lind, L. Love, P. Lloyd, J. Rowe, and F. G. Pin, "Design and control of a ship motion simulation platform from an energy efficiency perspective," *International Journal of Fluid Power*, vol. 10, no. 2, pp. 19–28, 2009.

[15] S. Fecht, "Inside the wave pool where the navy tests its warships." [Online] https://www.popularmechanics.com/military/navy-ships/a10407/inside-the-wave-pool-where-the-navy-tests-its-warships-16656545/, 2014.

[16] T. C. Smith, "Mask basin b'bank wave survey," tech. rep., Naval Surface Warfare Center Carderock Div Bethesda MD Hydromechanics Directorate, 1999.

[17] K. Slater and A. Fincham, "Surface gravity wave generator and wave pool," Sept. 11 2012. US Patent 8,262,316.

[18] S.-K. Ueng, D. Lin, and C.-H. Liu, "A ship motion simulation system," *Virtual Real.*, vol. 12, pp. 65–76, mar 2008.

[19] Y. Li and Q. Xu, "Kinematic analysis of a 3-prs parallel manipulator," *Robotics and Computer-Integrated Manufacturing*, vol. 23, no. 4, pp. 395 – 408, 2007.

[20] M.-S. Tsai, T.-N. Shiau, Y.-J. Tsai, and T.-H. Chang, "Direct kinematic analysis of a 3-prs parallel mechanism," *Mechanism and Machine Theory*, vol. 38, no. 1, pp. 71 – 83, 2003.

[21] X. Liu, J. Wang, T. Li, and G. Duan, "Parallel mechanisms with two or three degrees of freedom," *Tsinghua Science and Technology*, vol. 8, pp. 105–112, Feb 2003.

[22] Y. Li and Q. Xu, "Kinematics and stiffness analysis for a general 3-prs spatial parallel mechanism," 02 2019.

[23] K. Balaji and B. S. H. Khan, "Kinematic analysis and performance evaluation of novel PRS parallel mechanism," *IOP Conference Series: Materials Science and Engineering*, vol. 310, p. 012007, feb 2018.

[24] X. Li, D. Zhu, Z. Mei, and D. Jiang, "Kinematic analysis of 3-rps parallel mechanism," in *2017 2nd International Conference on Robotics and Automation Engineering (ICRAE)*, pp. 183–187, Dec 2017.

[25] H. Pendar, M. Vakil, and H. Zohoor, "Efficient dynamic equations of 3-rps parallel mechanism through lagrange method," in *IEEE Conference on Robotics, Automation and Mechatronics, 2004.*, vol. 2, pp. 1152–1157 vol.2, Dec 2004.

[26] J. Gallardo, H. Orozco, and J. M. Rico, "Kinematics of 3-rps parallel manipulators by means of screw theory," *The International Journal of Advanced Manufacturing Technology*, vol. 36, pp. 598–605, Mar 2008.

[27] X. Liu, T. Zhao, E. Luo, W. Chen, and Q. Pan, "Coupling 3-psr/psu 5-axis compensation mechanism for stabilized platform and its analysis," *Proceedings of the Institution of Mechanical Engineers, Part C: Journal of Mechanical Engineering Science*, vol. 227, no. 7, pp. 1619–1629, 2013.

[28] L.-W. Tsai, *Marine Observer's Handbook*. London, England: HMSO, 8th ed.

[29] T. Bewley, *Numerical Renaissance*. Renaissance Press, 2017.

[30] J. Diebel, "Representing attitude: Euler angles, unit quaternions, and rotation vectors," *Matrix*, vol. 58, no. 15-16, pp. 1–35, 2006.

[31] E. Darles, B. Crespin, D. Ghazanfarpour, and J.-C. Gonzato, "A survey of ocean simulation and rendering techniques in computer graphics," in *Computer Graphics Forum*, vol. 30, pp. 43–60, Wiley Online Library, 2011.

[32] A. Newell and V. Zakharov, "The role of the generalized phillips' spectrum in wave turbulence," *Physics Letters A*, vol. 372, no. 23, pp. 4230 – 4233, 2008.

[33] O. M. Phillips, "The equilibrium range in the spectrum of wind-generated waves," *Journal of Fluid Mechanics*, vol. 4, no. 4, p. 426–434, 1958.

[34] O. M. Phillips, "On the generation of waves by turbulent wind," *Journal of fluid mechanics*, vol. 2, no. 5, pp. 417–445, 1957.

[35] G. Castillo and C. Falcon, "Observation of phillips' spectrum in faraday waves," *arXiv preprint arXiv:1608.08961*, 2016.

[36] A. W. Browning, "A mathematical model to simulate small boat behaviour," *Simulation*, vol. 56, no. 5, pp. 329–336, 1991.

[37] T. Pérez and M. Blanke, "Simulation of ship motion in seaway," Tech. Rep. EE02037, Technical University of Denmark, 2001.